THE JOURNAL OF BIOLOGICAL CHEMISTRY
Vol. 277, No. 19, Issue of May 10, pp. 16419–16425, 2002

Printed in U.S.A.

Diffusional Mobility of the Cystic Fibrosis Transmembrane Conductance Regulator Mutant, ΔF508-CFTR, in the Endoplasmic Reticulum Measured by Photobleaching of GFP-CFTR Chimeras*

Received for publication, December 25, 2001, and in revised form, February 26, 2002
Published, JBC Papers in Press, February 27, 2002, DOI10.1074/jbc.M112361200

Peter M. Haggie‡, Bruce A. Stanton§, and A. S. Verkman‡¶

From the ‡Departments of Medicine and Physiology, Cardiovascular Research Institute, University of California, San Francisco, California 94143-0521 and §Dartmouth Medical School, Hanover, New Hampshire 03755-3835

Mutations in the cystic fibrosis transmembrane conductance regulator protein (CFTR) cause cystic fibrosis. The most common disease-causing mutation, ΔF508, is retained in the endoplasmic reticulum (ER) and is unable to function as a plasma membrane chloride channel. To investigate whether the ER retention of ΔF508-CFTR is caused by immobilization and/or aggregation, we have measured the diffusional mobility of green fluorescent protein (GFP) chimeras of wild type (wt)-CFTR and ΔF508-CFTR by fluorescence recovery after photobleaching. GFP-labeled ΔF508-CFTR was localized in the ER and wt-CFTR in the plasma membrane and intracellular membranes in transfected COS7 and Chinese hamster ovary K1 cells. Both chimeras localized to the ER after brefeldin A treatment. Spot photobleaching showed that CFTR diffusion (diffusion coefficient ~10^{-9} cm^2/s) was not significantly slowed by the ΔF508 mutation and that nearly all wt-CFTR and ΔF508-CFTR diffused throughout the ER without restriction. Stabilization of molecular chaperone interactions by ATP depletion produced remarkable ΔF508-CFTR immobilization (~50%) and slowed diffusion (6.5×10^{-10} cm^2/s) but had little effect on wt-CFTR. Fluorescence depletion experiments revealed that the immobilized ΔF508-CFTR in ATP-depleted cells remained in an ER pattern. The mobility of wt-CFTR and ΔF508-CFTR was reduced by maneuvers that alter CFTR processing or interactions with molecular chaperones, including tunicamycin, geldanamycin, and lactacystin. Photobleaching of the fluorescent ER lipid $diOC_4(3)$ showed that neither ER restructuring nor fragmentation during these maneuvers was responsible for the slowing and immobilization of CFTR. These results suggest that (*a*) the ER retention of ΔF508-CFTR is not due to restricted ER mobility, (*b*) the majority of ΔF508-CFTR is not aggregated or bound to slowly moving membrane proteins, and (*c*) ΔF508-CFTR may interact to a greater extent with molecular chaperones than does wt-CFTR.

The cystic fibrosis transmembrane conductance regulator protein (CFTR)[1] mediates transepithelial chloride transport across epithelial cells in the airways, intestine, pancreas, and sweat gland. Some mutations in CFTR cause the lethal genetic disease cystic fibrosis, which produces chronic lung infection, progressively impaired pulmonary function, and pancreatic insufficiency. The most common CFTR mutant, ΔF508-CFTR, is retained at the endoplasmic reticulum (ER) and consequently is unable to function as a plasma membrane chloride channel (1). Electrophysiological studies indicate that the ER-retained ΔF508-CFTR is at least partially functional in excised ER membranes (2). Further, growth of ΔF508-CFTR-expressing cells under non-physiological conditions (low temperature, Ref. 3 or with chemical chaperones, Ref. 4) indicates that under certain conditions ΔF508-CFTR can be transported to the plasma membrane and restore cell chloride permeability.

CFTR biosynthesis is an inefficient process. Newly synthesized wild type (wt)-CFTR and ΔF508-CFTR are folded into the ER membrane where they become core-glycosylated (5, 6). Only 20–30% of newly synthesized wt-CFTR is transported to the Golgi where complex glycosylation occurs, with the remaining protein ubiquinated and degraded by the proteasome (7, 8). Wild type CFTR exists initially in a protease-susceptible form ($t_{1/2}$ ~30 min) that becomes more stable upon transport from ER to Golgi ($t_{1/2}$ ~24 h), whereas ΔF508-CFTR is rapidly degraded ($t_{1/2}$ ~30 min) (5, 6). Inhibition of proteasome function results in the formation of aggresomes, which are detergent-insoluble, perinuclear protein aggregates common to many degenerative diseases (9–11).

CFTR folding in the ER appears to be facilitated by interactions with the cellular quality control machinery. Wild type CFTR and ΔF508-CFTR have been shown to interact with the molecular chaperones Hsc70, Hdj2, Hsp70, Hsp90, and calnexin but not with BiP or Grp94 (12–15). Recent data suggest that the Hsc70 co-chaperone CHIP (C-terminus of Hsc70-interacting protein) targets immature CFTR for proteasome-mediated degradation (16). Biochemical data indicate that calnexin and Hsp70 bind ΔF508-CFTR more avidly than wt-CFTR (12, 13). The differential processing of ΔF508-CFTR and wt-CFTR, however, is probably not accounted for by gross structural differences. Proteolytic cleavage experiments have suggested that the conformation of ΔF508-CFTR is similar to that of the early, relatively unstable form of wt-CFTR (17). *In vitro* folding studies of the isolated nucleotide binding domain 1 (containing

* This study was supported by National Institutes of Health Grants EB00415, DK43840, HL59198, DK35124, EY13574, and HL60288, Research Development Program Grant R613 from the Cystic Fibrosis Foundation (to A. S. V), and National Institutes of Health Grants DK45881 and DK34533 and a Research Development Program grant from the Cystic Fibrosis Foundation (to B. A. S). The costs of publication of this article were defrayed in part by the payment of page charges. This article must therefore be hereby marked "*advertisement*" in accordance with 18 U.S.C. Section 1734 solely to indicate this fact.

¶ To whom correspondence should be addressed: 1246 Health Sciences East Tower, Cardiovascular Research Inst., University of California, San Francisco, San Francisco, CA 94143-0521. Tel.: 415-476-8530; Fax: 415-665-3847; E-mail: verkman@itsa.ucsf.edu.

[1] The abbreviations used are: CFTR, cystic fibrosis transmembrane conductance regulator; ER, endoplasmic reticulum; GFP, green fluorescent protein; wt, wild type; CHO, Chinese hamster ovary; BFA, brefeldin A; N.A., numerical aperture; VSVG, vesicular stomatitis virus G protein; AQP, aquaporin; $diOC_4(3)$, 3,3′-dibutyloxacarbocyanine iodide; FLIP, fluorescence loss in photobleaching.

the phenylalanine 508 residue) support the view that the ΔF508 mutation does not affect structure (18, 19) but may affect folding kinetics.

Here we have used fluorescence recovery after photobleaching to measure the diffusional mobility of wt-CFTR and ΔF508-CFTR at the ER to investigate whether ΔF508-CFTR immobilization or interaction with chaperones is responsible for its ER retention. Several mechanisms have been proposed to explain the failure of ΔF508-CFTR to be exported from the ER: immobilization of ΔF508-CFTR, potentially by association with chaperones or by self-aggregation; efficient ΔF508-CFTR recycling from the Golgi; and/or failure of the ER export machinery to recognize ΔF508-CFTR. Photobleaching measurements were done on cells expressing green fluorescent protein (GFP) chimeras of wt-CFTR and ΔF508-CFTR; a series of maneuvers was used to probe for interactions with CFTR processing machinery. It was shown previously that GFP fusion to the N terminus of CFTR did not effect CFTR localization, processing, or function (9, 20–22). We used photobleaching previously to quantify aqueous phase rheology in cellular and organellar compartments (23–25) and to investigate protein-protein interactions of aquaporin (AQP) water channels in the ER and plasma membranes (26, 27). We find here that the ER retention of ΔF508-CFTR is not due to immobilization, aggregation, or binding to slow moving membrane components; however, a greater fraction of ΔF508-CFTR than wild type CFTR interacted with molecular chaperones after ATP depletion, and inhibition of CFTR processing by a proteasome inhibitor resulted in CFTR aggregation and immobilization.

EXPERIMENTAL PROCEDURES

Cell Culture, Plasmids, Transfection, and Treatments—COS7 (ATCC CRL-1651) and CHO-K1 (ATCC CCL-61) cells (obtained from the University of California, San Francisco Cell Culture Facility) were cultured in DMEH-21 and Ham's F12 media, respectively, supplemented with 10% fetal bovine serum, 100 units/ml penicillin and 100 μg/ml streptomycin at 37 °C in a 5% CO_2/95% air atmosphere. Cells were grown on 18-mm diameter glass coverslips in 12-well plates. Cells were transiently transfected with plasmid DNA using 6 μl of lipofectamine (Invitrogen) and 1 μg of plasmid DNA according to the manufacturer's instructions.

cDNA encoding wt-CFTR was fused downstream of the enhanced GFP (CLONTECH) as described previously, and the ΔF508 mutation was introduced by site-directed mutagenesis (20, 22). A glycosylation-null mutant of GFP-wt-CFTR, in which asparagine residues were replaced by glutamines at positions 894 and 900, was also generated by site-directed mutagenesis. For GFP expression in the ER lumen, the GFP sequence was flanked by an N-terminal preprolactin leader sequence and a C-terminal KDEL motif (25). For GFP expression in the cytoplasm, the coding region of pEGFP (CLONTECH) was ligated into pcDNA3.1 as a *Hin*dIII/*Eco*RI fragment.

Photobleaching experiments were performed 2–3 days after transfection for CFTR-transfected cells and 1–2 days after transfection for cytoplasmic or ER-targeted unconjugated GFP. For most experiments GFP-CFTR-transfected cells were treated with brefeldin A (BFA) by 16–24 h of incubation at 5 μg/ml at 37 °C in the CO_2 incubator. For ATP depletion, cells were incubated in phosphate-buffered saline containing 6 mM 2-deoxyglucose and 0.02% sodium azide at 37 °C for 30 min or 1 h. Geldanamycin (Calbiochem) was used at 0.1 μg/ml for 90 min (14) and tunicamycin (Calbiochem) at 5 μg/ml for 20 h. Clasto-lactacystin β-lactone (the active form of lactacystin, Sigma) was used at 6 μM for 1.5, 6, or 14 h. In heat shock experiments, cells were incubated at 42 °C for 1 h followed by 16–20 h recovery at 37 °C. Paraformaldehyde (for GFP-CFTR immobilization) was used at 4% for 30 min in phosphate-buffered saline at 23 °C. ER membranes in untransfected cells (subjected to various treatments above) were fluorescently labeled with 3,3′-dibutyloxacarbocyanine iodide ($diOC_4(3)$, Molecular Probes) by incubation for 10 min with 10 μM dye in phosphate-buffered saline at 37 °C. In some experiments transfected cells were identified by their green fluorescence prior to $diOC_4(3)$ labeling, and those cells were photobleached. The relatively small amount of GFP had little effect on the recovery of the much brighter and more rapidly diffusing $diOC_4(3)$.

Fluorescence Recovery after Photobleaching—For spot photobleaching, an argon ion laser beam (488 nm, Innova 70–4, Coherent) was modulated by an acousto-optic modulator and the first-order beam was directed onto cells through an oil immersion (Nikon fluor) objective lens (×40, numerical aperture (N.A.) 1.3; ×60, N.A. 1.4; or ×100, N.A. 1.4) using an inverted epifluorescence microscope. To visualize cells and to select cellular regions to be bleached, full-field epi-illumination was accomplished using the expanded zero-order laser beam directed onto the objective lens by a fiber optic. The beam was reflected onto the objective by a dichroic mirror (510 nm), and emitted fluorescence was filtered by serial 530 ± 15 nm bandpass and 515 nm longpass filters. Emitted fluorescence was detected by a photomultiplier and digitized by a 14-bit analog-to-digital converter. The photomultiplier was transiently gated off during the bleach pulse. Fluorescence was sampled over 200 ms before the bleach pulse, then at rates of up to 1 MHz. For measurement of slow recoveries, an electronic shutter was used to collect fluorescence at 1 Hz, averaging 10,000 acquisitions during the shutter open time of 20 ms.

For photobleaching experiments with image detection, a Leitz upright microscope with a cooled CCD camera detector (Photometrics) was used to record full-field epifluorescence images. An electronically shuttered bleach beam from the argon laser (488 nm) was directed onto the sample (from below) using a Nikon ×25 long working-distance air objective. Cells were viewed (from above) using an oil immersion ×60 objective (N.A. 1.4) and GFP filter set (HQ filters, Chroma). Software was written (in LabVIEW, National Instruments) to coordinate the bleach pulse, illumination and camera shutters, and image acquisition. Fluorescence loss in photobleaching (FLIP) experiments were performed using the same apparatus in which repeated laser photobleaching was performed with specified delays between bleach pulses.

All photobleaching experiments were done at 37 °C. Cultured cells were mounted in custom built perfusion chambers designed to fit a PDMI-2 microincubator (Harvard Apparatus) controlled by a TC-201A temperature regulator (Harvard Apparatus). Objective lens temperature was also maintained at 37 °C using a lens thermoregulator (Bioptechs Inc., Butler, PA). For maneuvers on GFP-CFTR-expressing cells, single recovery curves from 5–12 different cells were averaged to generate a single averaged recovery curve, and this was repeated 4–10 times using different coverslips. For cytoplasmic GFP and ER-targeted GFP-expressing cells, each averaged recovery curve was generated from 10 individual recoveries, each from a different cell. For $diOC_4(3)$ measurements, averaged recovery curves were generated from the average of 5–8 cells. Results are reported as means ± S.E. for the number of different coverslips, and representative averaged recovery curves from single coverslips are shown in figures for the reader to evaluate curve shape and signal-to-noise ratio. Statistical analysis was performed by analysis of variance against control conditions, and values of $p < 0.05$ were considered significant.

Analysis of Photobleaching Recovery Data—Spot photobleaching recovery curves were analyzed as described in Levin *et al*. (27). Briefly, recovery half-times ($t_{½}$), the time for fluorescence to recover by 50% due to diffusion, were determined from fluorescence recovery curves, $F(t)$, by non-linear regression. Fluorescence recovery curves were taken to be a combination of reversible (as determined from fixed cell analysis) and irreversible (due to diffusion) processes, $F(t) = a_1(F(t)_{\text{reversible}} + a_2(F(t)_{\text{irreversible}})$ where $a_1 + a_2 = 1$. The diffusion-mediated recovery was fitted using the semiempirical equation: $F(t)_{\text{irreversible}} = F_0 + (F_0 + R(F_{inf} - F_0))(t/t_{½})/(1 + (t/t_{½}))$ where F_0 is prebleach fluorescence, F_{inf} is fluorescence at infinite time, and R is the fractional fluorescence recovery. Absolute diffusion coefficients were calculated from $t_{½}$ using a mathematical model of ER diffusion (25, 28).

RESULTS

The diffusion of wt-CFTR and ΔF508-CFTR in the ER of living cells was determined using GFP as a fluorescent reporter (Fig. 1*A*). Transfection of COS7 and CHO cells with the GFP-wt-CFTR chimera showed GFP localization to the plasma membrane and intracellular membranes (including Golgi and ER) but exclusively to the ER after BFA treatment (Fig. 1*B*). The GFP-ΔF508-CFTR chimera was seen in an ER-like pattern without or after BFA treatment (Fig. 1*C*). Similar patterns of ER staining were observed in COS7 and CHO cells transfected with ER-localized (aqueous phase) GFP or stained with the fluorescent ER lipid probe $diOC_4(3)$ (not shown).

Photobleaching experiments with image detection were done to evaluate the gross mobility of GFP-CFTR chimeras in BFA-

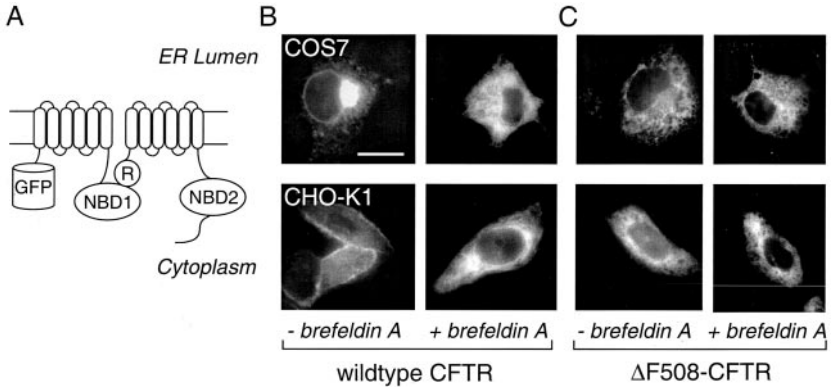

FIG. 1. **GFP-CFTR expression in transiently transfected COS7 and CHO cells.** *A*, GFP-CFTR construct showing CFTR fused downstream of the GFP reporter. *B*, fluorescence micrographs of transiently transfected COS7 and CHO cells expressing GFP-wt-CFTR without (*left*) and after (*right*) BFA treatment. *C*, fluorescence micrographs of cells expressing GFP-ΔF508-CFTR. *Scale bar*, 10 μm.

treated COS7 (Fig. 2*A*) and CHO (Fig. 2*B*) cells. A large region of the cell, ~5 μm in diameter (marked by *cross-hairs*), was bleached by the laser pulse, and fluorescence recovery was recorded by serial imaging. In each case a darkened region is seen immediately postbleach (*t = 0 s*). Recovery into this bleached region is diffusive in nature from the edges of the bleach spot inward and appears to be nearly complete. The kinetics of fluorescence recovery were qualitatively similar for cells expressing wt-CFTR and ΔF508-CFTR and in both cell types. In each case the fluorescence recovery was > 80% complete as determined from the ratio of fluorescence intensity in the bleach spot to the whole cell immediately after *versus* 4 min after the bleach. Quantitative spot photobleaching was done in the brighter COS7 cells.

Fig. 3*A* shows spot photobleaching of GFP-labeled wt-CFTR (*top*) and ΔF508-CFTR (*bottom*) using a ×60 oil immersion objective to produce a small spot (~1.2-μm diameter) in which GFP fluorescence was bleached to ~50% of its initial value. To distinguish between processes that produce irreversible photobleaching (authentic GFP diffusion) from those that produce reversible photobleaching (from triplet-state relaxation or other photophysical phenomena), fluorescence recovery was measured in fixed cells (Fig. 3*B*) and using different spot sizes (Fig. 3*C*). As found in prior photobleaching studies (26, 27), the fluorescence recovery remaining after fixation represents reversible (diffusion-independent) photobleaching because fixation abolishes diffusion. Fig. 3*B* (*top curve*) shows a small component (5–10%) of reversible photobleaching with ~1-s exponential time constant. Similar recoveries were found under the same photobleaching conditions for unconjugated GFP in cytoplasm (*middle curve*) and aqueous phase (unconjugated) GFP in the ER lumen (*bottom curve*). As expected for reversible fluorescence recovery, the recovery rates did not depend on spot size (not shown). Fig. 3*C* shows that (in unfixed cells) the fluorescence recovery was spot size-dependent as expected for diffusive processes, because the recovery time for a larger spot increases approximately with the square of the spot diameter. Using a regression procedure to determine ($t_{1/2}$) for irreversible fluorescence recovery (see "Experimental Procedures"), $t_{1/2}$ values for GFP-wt-CFTR were 1040 ± 60 ms (100×), 3.0 ± 0.4 s (60×), and 4.9 ± 0.2 s (40×) (n = 4–10 sets of measurements). The $t_{1/2}$ values for GFP-ΔF508-CFTR (in BFA-treated cells) were 1170 ± 120 ms (100×), 3.3 ± 0.5 s (60×), and 6.4 ± 0.3 s (40×) (n = 4–10). The relative $t_{1/2}$ are as expected for a diffusive process.

To determine absolute diffusion coefficients, comparative photobleaching measurements were done for the GFP-labeled CFTR chimeras (Fig. 3*A*) and for soluble GFP in the ER lumen. From a series of experiments shown in Fig. 3*A*, $t_{1/2}$ measured using a ×60 objective were 3.0 ± 0.4 s (wt-CFTR), 3.3 ± 0.5 s (ΔF508-CFTR, +BFA), and 3.3 ± 0.6 s (ΔF508-CFTR, −BFA) (n = 5–10 sets of experiments). Fig. 3*D* (*top*) shows the substantially faster fluorescence recovery of soluble GFP in the ER lumen of COS7 cells ($t_{1/2}$, 60 ± 4 ms; n = 12). This value was similar to that measured in CHO-K1 cells under identical conditions ($t_{1/2}$, 65 ± 4 ms; n = 6, not shown). The absolute diffusion coefficient for luminal GFP in COS7 cells was computed using a simple model to correct for ER geometric effects (28) as (6.0 ± 0.5) × 10^{-8} cm^2/s, similar to that previously measured in CHO cells (25) and LLC-PK1 cells (27).

Fig. 3*D* (*middle*) summarizes diffusion coefficients for the GFP-chimeras. There was no significant effect of the ΔF508 mutation on CFTR diffusion and/or of BFA treatment on ΔF508-CFTR mobility. Fig. 3*D* (*bottom*) summarizes the percentage of mobile GFP, determined from the completeness of the fluorescence recovery at long times. GFP-wt-CFTR fluorescence recovered almost completely (92 ± 2%, n = 10), whereas GFP-ΔF508-CFTR recovery in BFA-treated and untreated cells was slightly though significantly smaller (85 ± 2% and 82 ± 1%).

To investigate interactions of wt-CFTR and ΔF508-CFTR with elements of the ER quality control machinery, we used a series of maneuvers to modulate molecular chaperone interactions. Fig. 4*A* shows wt-CFTR mobility after ATP depletion (a maneuver that increases interactions between CFTR and chaperones in the ER), which was produced by 30 min of incubation with 6 mM 2-deoxyglucose and 0.02% sodium azide (*top curve*). The diffusion coefficient of GFP-wt-CFTR was similar to control conditions, (10.6 ± 0.9) × 10^{-10} cm^2/s (n = 7), and the percentage recovery was reduced significantly to 80 ± 2%. The diffusion coefficient of GFP-ΔF508-CFTR was reduced significantly after a 30-min ATP depletion to (6.6 ± 0.5) × 10^{-10} cm^2/s (n = 5) (Fig. 4*A*, *bottom curve*), and substantially more GFP-ΔF508-CFTR became immobilized (mobile percentage, 55 ± 5%). ATP depletion for 60 min had no further effect. Table I summarizes averaged diffusion coefficients and percentages of mobile GFP. To investigate whether the reduced ΔF508-CFTR mobility in ATP-depleted cells was related to restructuring or fragmentation of the ER, the mobility of the fluorescent ER membrane marker $diOC_4(3)$ was measured. Fig. 4*B* shows that diffusion of $diOC_4(3)$ was essentially complete with a diffusion coefficient of (2.4 ± 0.1) × 10^{-8} cm^2/s (n = 10). $diOC_4(3)$ diffusion was unaffected by BFA treatment ((2.4 ± 0.1) × 10^{-8} cm^2/s, n = 5, *middle curve*) or ATP depletion ((2.7 ± 0.3) × 10^{-8} cm^2/s, n = 4, *bottom curve*). Further, photobleaching of transfected cells expressing GFP-labeled wild type CFTR or ΔF508-CFTR and subsequently labeled with $diOC_4(3)$ *in situ* showed that the expression of GFP-CFTR chimeras did not affect ER structure or fluidity (not shown). Image photobleaching experiments similar to those shown in Fig. 2 were also performed on $diOC_4(3)$-labeled cells (not shown), and it was demonstrated that ATP depletion did not alter ER continuity or gross structure.

To identify the cellular location of the immobilized GFP-ΔF508-CFTR in ATP-depleted cells, fluorescence loss in photobleaching (FLIP) experiments were performed (Fig. 4*C*). A

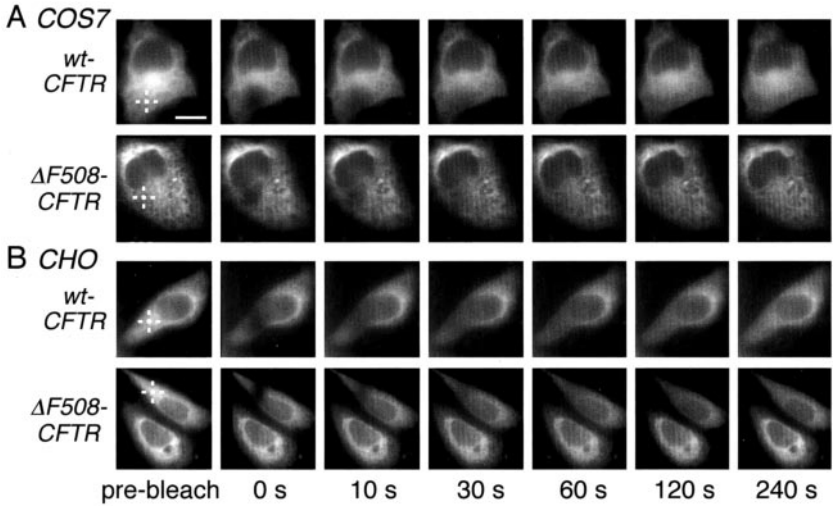

FIG. 2. **Photobleaching of GFP-CFTR chimeras in transiently transfected COS7 (*A*) and CHO (*B*) cells.** Photobleaching with image detection in cells expressing GFP-labeled wt-CFTR and ΔF508-CFTR (after BFA treatment). Images are shown before bleaching, with the bleach spot indicated by *white crosshairs*, and at the indicated times after the bleach pulse. All experiments were done at 37 °C. Each image series is one set of experiments representative of 4–8. *Scale bar*, 10 μm.

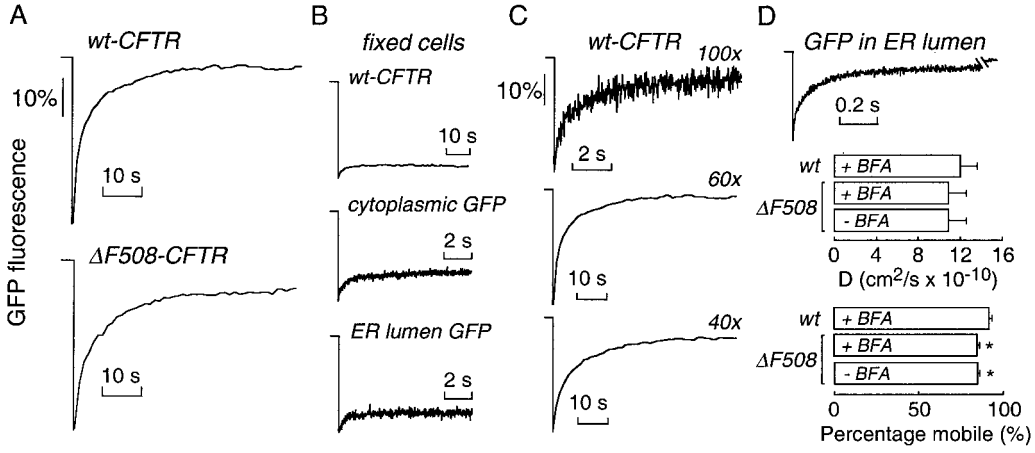

FIG. 3. **Quantitative spot photobleaching of the diffusion of GFP-labeled wt-CFTR and ΔF508-CFTR at the ER.** *A*, spot photobleaching of cells expressing wt-CFTR (*top*) and ΔF508-CFTR (*bottom*), measured using a ×60 oil immersion objective. Bleach time was 200–500 μs. Each curve is the average of 10 fluorescence recovery experiments, each done on a different cell. *B*, spot photobleaching of paraformaldehyde-fixed cells expressing GFP-labeled wt-CFTR (*top*), cytoplasmic (unconjugated) GFP (*middle*), and ER-lumen aqueous phase GFP (*bottom*). Measurements done with the ×60 objective. *C*, spot photobleaching of GFP-labeled wt-CFTR measured using indicated objectives. Bleach time was adjusted to give 40–50% bleach. *D*, spot photobleaching of soluble GFP in the ER lumen (*top*). Summary of absolute diffusion coefficients (*D*, *middle*) and percentage fluorescence recoveries (*bottom*) for the GFP-CFTR chimeras (S.E., $n = 5$–10 sets of experiments, *, $p < 0.005$).

fixed spot in the cell was repetitively bleached with delays between each bleach pulse to permit diffusion of unbleached GFP-labeled CFTR into the location of the bleach spot. Under these conditions GFP-wt-CFTR freely diffused throughout the ER with ~10% of cell fluorescence remaining after 35 bleach pulses (*top*). In contrast, a substantial amount of fluorescence remained after bleaching of GFP-ΔF508-CFTR in ATP-depleted cells (*bottom*) with the remaining fluorescence having an ER pattern. These findings suggest that ATP depletion does not alter ER continuity or gross structure and that the immobilization of ΔF508-CFTR in ATP-depleted cells results from interactions with ER proteins.

Additional maneuvers were carried out to modulate putative CFTR interactions with molecular chaperones and elements of protein processing and degradation (Fig. 5 and Table I). Heat shock, which nonspecifically up-regulates the expression of molecular chaperones, produced small reductions in the diffusion coefficients and percentage mobilities of wt-CFTR and ΔF508-CFTR (Fig. 5, *top curves*). Proteasome inhibition by lactacystin resulted in mild slowing and immobilization of wt-CFTR and ΔF508-CFTR after 6 h of incubation (*second curves*), with complete immobilization after 14 h (*third curves*). GFP was seen in an ER pattern at 6 h but was concentrated in aggresomes at 14 h (not shown). The ansamycin compound geldanamycin, which disrupts associations with Hsp90, caused comparable slowing of wt-CFTR and ΔF508-CFTR with somewhat greater immobilization of ΔF508-CFTR (*fourth curves*). Last, the role of glycosylation was investigated by incubation with tunicamycin (to inhibit addition of oligosaccharide chains), using a glycosylation-null mutant of wt-CFTR (asparagines 894 and 900 replaced by glutamines). Somewhat more immobilization of ΔF508-CFTR than wt-CFTR was found with tunicamycin (*fifth curves*). Although the glycosylation-null mutant of wt-CFTR expressed poorly and a substantial proportion of fluorescence was associated with aggresomes, the mobility of ER-associated CFTR could be measured in some cells and was found to be similar to that produced by tunicamycin (*sixth curve*).

As was done for the ATP depletion experiments, the diffusion of the ER marker $diOC_4(3)$ was measured in transfected cells to establish that ER restructuring or fragmentation was not responsible for reduced CFTR mobility. The diffusion of $diOC_4(3)$ in cells that were heat-shocked or treated with lactacystin, geldanamycin, or tunicamycin was essentially complete (>96% mobile) and similar to that measured in control cells, with diffusion coefficients of 2.2–2.7 $\times 10^{-8}$ cm^2/s ($n = 4$ for each treatment, data not shown).

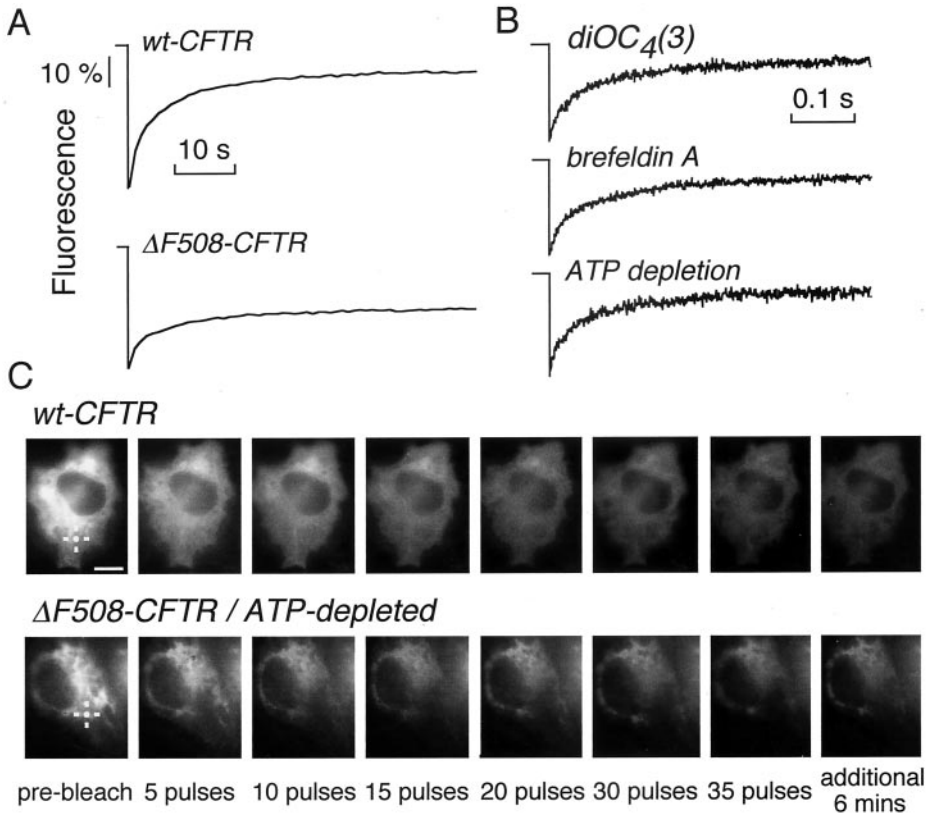

FIG. 4. **Slowed GFP-ΔF508-CFTR diffusion after ATP depletion.** *A*, photobleaching after cellular ATP depletion produced by a 30-min incubation with 6 mM 2-deoxyglucose and 0.02% sodium azide (×60 objective). *B*, photobleaching of the ER lipid probe $diOC_4(3)$ in control, BFA-treated, and ATP-depleted cells (×100 objective). *C*, fluorescence depletion experiments of GFP-wt-CFTR under control conditions (*top*) and of GFP-ΔF508-CFTR after ATP depletion (*bottom*). Images shown before bleaching, with the bleach spot indicated by *white cross-hairs*, and after the indicated number of bleach pulses. *Scale bar*, 10 μm.

TABLE I
Diffusion coefficients (D) and mobilities of wt- and ΔF508-CFTR

Data as mean ± S.E. (n = 4–10 sets of measurements, each measurement the average of 5–12 recovery curves from different cells) for indicated maneuvers (see "Experimental Procedures").

		Mobility		*D*	
		wt-CFTR	ΔF508-CFTR	wt-CFTR	ΔF508-CFTR
		%		$cm^2/s \times 10^{-10}$	
Control	+BFA	92 ± 2	85 ± 2[b]	12 ± 1.6	11.1 ± 1.6
	−BFA	not done	82 ± 1	not done	11.1 ± 2.0
ATP depletion	30 min	80 ± 2[a]	55 ± 5[a,b]	10.6 ± 0.9	6.7 ± 0.5[a,b]
	60 min	78 ± 2[a]	50 ± 2[a,b]	8.6 ± 1.2	6.5 ± 0.4[a]
Heat shock		86 ± 2	81 ± 1	10.0 ± 2.0	7.5 ± 1.1
Lactacystin	1.5 h	78 ± 7[a]	74 ± 5	4.6 ± 1.0[a]	4.3 ± 1.0[a]
	6 h	80 ± 3[a]	66 ± 9[a]	6.1 ± 0.8[a]	4.7 ± 0.4[a]
	14 h	immobile	immobile	immobile	immobile
Geldanamycin		83 ± 3[a]	69 ± 3[a,b]	4.9 ± 0.9[a]	4.3 ± 0.6[a]
Tunicamycin		81 ± 1[a]	68 ± 3[a,b]	8.2 ± 1.0[a]	5.4 ± 0.6[a]
Glycosylation null		66 ± 5[a]	not done	5.6 ± 1.0[a]	not done

[a] $p < 0.05$ compared to control.
[b] $p < 0.05$ comparing wt-CFTR vs. ΔF508-CFTR for individual maneuvers (analysis of variance).

DISCUSSION

This study has shown that although ΔF508-CFTR is retained in the ER, it diffuses at a comparable rate to wt-CFTR in BFA-treated cells. Similar observations were made for the T126M mutant of AQP2 (a water channel that is partially misfolded and similarly retained in the ER, Ref. 27) and for a temperature-sensitive folding mutant of the vesicular stomatitis virus G protein (29). Therefore, slowed or restricted ΔF508-CFTR mobility in the ER cannot account for its failure to be exported. Efficient recycling from the Golgi or failure to be recognized by the ER export machinery remain possible explanations for the ER localization of ΔF508-CFTR. The observation of small amounts of ΔF508-CFTR in post-ER membranes suggests that efficient recycling may be responsible for the retention of ΔF508-CFTR in the ER (30).

The small immobile pool of ΔF508-CFTR and the substantial immobilization after ATP depletion suggest that a greater fraction of ΔF508-CFTR interacts with molecular chaperones than does wt-CFTR. Approximately 50% of ΔF508-CFTR was immobile after ATP depletion, with only minor effects on the mobility of wt-CFTR. The simplest interpretation of this finding is that ATP depletion, which stabilizes protein interactions with molecular chaperones, is able to reveal ΔF508-CFTR interactions that are not observable under normal conditions. As discussed in the Introduction, ΔF508-CFTR structure is thought to be similar to that of an early intermediate of wt-CFTR, and biochemical evidence supports ΔF508-CFTR associations with molecular chaperones.

Additional maneuvers were performed to investigate specific interactions between wt-CFTR and ΔF508-CFTR and the cellular protein processing machinery. Inhibition of *N*-linked glycosylation by tunicamycin resulted in significant slowing and immobilization of both wt-CFTR and ΔF508-CFTR, similar to findings for the VSVG glycoprotein (29). Similar results were

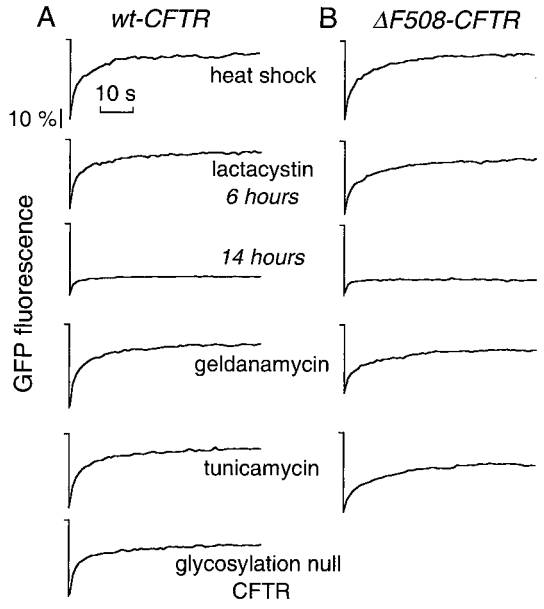

FIG. 5. **Effect of putative modulators of molecular chaperone interactions on the ER mobility of GFP-wt-CFTR and GFP-ΔF508-CFTR.** Photobleaching experiments were done on cells expressing wt-CFTR (*A*) and ΔF508-CFTR (*B*) using a ×60 objective as in Fig. 4*A*. Recovery curves are the average of 5–12 individual measurements, each from a single cell. Maneuvers are described under "Experimental Procedures" and include: heat shock, 1 h of incubation at 42 °C followed by 16–20 h of recovery at 37 °C; lactacystin, 6 μM for 6 and 14 h; geldanamycin, 0.1 μg/ml for 90 min; tunicamycin, 5 μg/ml for 20 h; and glycosylation-null mutant of GFP-wt-CFTR. For curves shown, the fitted absolute diffusion coefficient (in $cm^2/s \times 10^{-10}$) and percentage recoveries were the following: 9.0, 84% (heat shock, wt); 8.2, 83% (heat shock, ΔF508-CFTR); 6.2, 81% (lactacystin 6 h, wt); 5.0, 6.7% (lactacystin 6 h, ΔF508-CFTR); 7.0, 74% (geldanamycin, wt); 4.0, 63% (geldanamycin, ΔF508-CFTR); 6.7, 81% (tunicamycin, wt); 5.2, 61% (tunicamycin, ΔF508-CFTR); 6.0, 63% (glycosylation-null). See Table I for summary of fitted mobilities and diffusion coefficients.

found with a glycosylation-null wt-CFTR mutant, which was poorly expressed in the plasma membrane as determined by biotinylation studies (not shown). Protein glycosylation can facilitate folding, sorting, and quality control (31). Our data are thus consistent with a role for glycosylation in CFTR folding. Proteasome inhibition causes the accumulation of deglycosylated wt-CFTR and ΔF508-CFTR in detergent-insoluble, high molecular weight aggregates (9, 32). Consistent with the observations here, Bebök *et al*. (32) demonstrated an association between the Sec61 translocation system and CFTR that was enhanced by proteasome inhibition. After prolonged (14 h) incubation with lactacystin, wt-CFTR and ΔF508-CFTR were found in aggresomes (9, 10). Aggresomes are vimentin-enclosed, pericentriolar, electron-dense structures that contain aggregates of misfolded, often ubiquinated proteins associated with molecular chaperones and proteasomes. As expected, the GFP-CFTR chimeras were completely immobile in aggresomes.

Inhibition of interaction between Hsp90 and CFTR by geldanamycin also slowed the diffusion of wt-CFTR and ΔF508-CFTR, with greater immobilization of ΔF508-CFTR. Geldanamycin has been shown to disrupt interactions of Hsp90 and CFTR, increasing the degradation rates of wt-CFTR and ΔF508-CFTR (14). Hsp90 has thus been proposed to have a potential role in protecting CFTR from rapid degradation. The relative immobilization of wt-CFTR and ΔF508-CFTR after geldanamycin treatment supports a role of Hsp90 for CFTR processing. As suggested for VSVG by Nehls *et al*. (29), we believe that the physical state of wt-CFTR and ΔF508-CFTR after perturbation of CFTR processing by tunicamycin or geldanamycin may be different from that produced by ATP depletion. The slowing and immobilization of CFTR by ATP depletion may represent CFTR interactions with molecular chaperones existing in large complexes (33), whereas the immobilization after tunicamycin and geldanamycin, or molecular deglycosylation, may represent CFTR self-aggregation. Because of the logarithmic relationship between molecular radius and diffusion rate for a protein in a bilayer, substantial aggregates (10–100 units) must be formed to significantly slow diffusion. The similar responses of wt-CFTR and ΔF508-CFTR to some of the pharmacological maneuvers are consistent with the intrinsically inefficient folding of wt-CFTR, which when compared with P-glycoprotein (another member of the ABC cassette family) is poorly folded.

The diffusion coefficient for CFTR diffusional mobility in the ER, $\sim 10 \times 10^{-10}$ cm^2/s, is within the range of other ER membrane proteins that have been studied. The membrane water channel AQP2 (retained in the ER with BFA) and the ER-retained mutant AQP2-T126M have diffusion coefficients of $2.6–3.0 \times 10^{-10}$ cm^2/s (27). Cytochrome P450 2C2, an intrinsic ER protein, has a diffusion coefficient of 5.8×10^{-10} cm^2/s (34). VSVG in its native and misfolded states and two ER resident transmembrane proteins (lamin B receptor and the β-subunit of the signal recognition particle receptor) have diffusion coefficients of $26–50 \times 10^{-10}$ cm^2/s, depending upon temperature (29). Two Golgi resident transmembrane proteins (galactosyltransferase and the KDEL receptor) retained in the ER with BFA have diffusion coefficients of $21–48 \times 10^{-10}$ cm^2/s, depending upon cell type and temperature (29, 35). The diffusion coefficient of the ER-retained MHC class 1 molecule $H2L^d$ is $20–46 \times 10^{-10}$ cm^2/s and that of TAP1 (transporter associated with antigen presentation 1) is 12×10^{-10} cm^2/s (36). The variation in these diffusion coefficients probably reflects different protein sizes, interactions with ER and cytoplasmic proteins, and ER composition in different cells.

In summary, the photobleaching data provide the following evidence: (*a*) the ER retention of ΔF508-CFTR is not due to restricted ER mobility, (*b*) the majority of ΔF508-CFTR is not aggregated or bound to slowly moving membrane proteins, and (*c*) ΔF508-CFTR may interact to a greater extent with molecular chaperones than does wt-CFTR. Measurements of ER membrane protein diffusion provide a unique *in vivo* approach to study protein-protein associations that complements classical biochemical and 2-hybrid methods.

Acknowledgment—We thank Katherin Karlson for assistance with the generation of the glycosylation-null mutant of EGFP-CFTR.

REFERENCES

1. Cheng, S. H. Gregory, R. J., Marshall, J., Paul, S., Souza, D. W., White, G. A., O'Riordan, C. R., and Smith, A. E. (1990) *Cell* **63,** 827–834
2. Pasyk, E. A., and Foskett, J. K. (1995) *J. Biol. Chem.* **270,** 12347–12350
3. Denning, G. M., Anderson, M., Amara, J., Marshall, J., Smith, A., and Welsh, M. (1992) *Nature* **358,** 761–764
4. Brown, C. R., Hong-Brown, L. Q., Biwersi, J., Verkman, A. S., and Welch, W. J. (1996) *Cell Stress Chaperones* **1,** 117–125
5. Ward, C. L., and Kopito, R. R. (1994) *J. Biol. Chem.* **269,** 25710–25718
6. Lukacs, G. L., Mohamed, A., Kartner, N., Chang, X. B., Riordan, J. R., and Grinstein, S. (1994) *EMBO J.* **13,** 6076–6086
7. Ward, C. L., Omura, S., and Kopito, R. R. (1995) *Cell* **83,** 121–127
8. Jensen, T. J, Loo, M. A., Pind, S., Williams, D. B., Goldberg, A. L., and Riordan, J. R. (1995) *Cell* **83,** 129–135
9. Johnston, J. J., Ward, C. L., and Kopito, R. R. (1998) *J. Cell Biol.* **143,** 1883–1893
10. Wigley, W. C., Fabunmi, R. P., Lee, M. G., Marino, C. R., Muallem, S., DeMartino, G. N., and Thomas, P. J. (1999) *J. Cell Biol.* **145,** 481–490
11. Kopito, R. R. (2000) *Trends Cell Biol.* **10,** 524–530
12. Yang, Y., Janich, S., Cohn, J. A., and Wilson, J. M. (1993) *Proc. Natl. Acad. Sci. U. S. A.* **90,** 9480–9484
13. Pind, S., Riordan, J. R., and Williams, D. B. (1994) *J. Biol. Chem.* **269,** 12784–12788
14. Loo, M. A., Jensen, T. J., Cui, L., Hou, Y. X., Chang, X. B., and Riordan, J. R. (1998) *EMBO J.* **17,** 6879–6887
15. Meacham, G. C., Lu, Z., King, S., Sorscher, E., Tousson, A., and Cyr, D. M. (1999) *EMBO J.* **18,** 1492–1505
16. Meacham, G. C., Patterson, C., Zhang, W., Younger, J. M., and Cyr, D. M.

(2001) *Nat. Cell Biol.* **3,** 100–10522
17. Zhang, F., Kartner, N., and Lukacs, G. L. (1998) *Nat. Struct. Biol.* **5,** 180–183
18. Qu, B. H., and Thomas, P. J. (1996) *J. Biol. Chem.* **271,** 7261–7264
19. Qu, B. H., Strickland, E. H., and Thomas, P. J. (1997) *J. Biol. Chem.* **272,** 15739–15744
20. Moyer, B. D., Loffing, J., Schwiebert, E. M., Loffing-Cueni, D., Halpin, P. A., Karlson, K. H., Ismailov, I. I., Guggino, W. B., Langford G. M., and Stanton, B. A. (1998) *J. Biol. Chem.* **273,** 21759–21768
21. Moyer, B. D., Denton, J., Karlson, K. H., Reynolds, D., Wang, S., Mickle, J. E., Cutting, G. R., Guggino, W. B., Li, M., and Stanton, B. A. (1999) *J. Clin. Invest.* **104,** 1351–1361
22. Loffing-Cueni, D., Loffing, J., Shaw, C., Taplin, A.-L. M., Govindan, M., Stanton, C. R., and B. A. Stanton. (2001) *Am. J. Physiol.* **281,** C1889–C1897
23. Seksek, O., Biwersi, J., and Verkman, A. S. (1997) *J. Cell Biol.* **138,** 131–142
24. Partikian, A., Ölveczky, B., Swaminathan, R., Li., Y., and Verkman, A. S. (1998) *J. Cell Biol.* **140,** 821–829
25. Dayel, M. J., Hom, E. F., and Verkman, A. S. (1999) *Biophys. J.* **76,** 2843–2851
26. Umenishi, F., Verbavatz, J. M., and Verkman, A. S. (2000) *Biophys. J.* **78,** 1024–1035
27. Levin, M. H., Haggie, P. M., Vetrivel, L., and Verkman, A. S. (2001) *J. Biol. Chem.* **276,** 21331–21336
28. Ölveczky, B. P., Periasamy, N., and Verkman, A. S. (1997) *Biophys. J.* **73,** 2836–2847
29. Nehls, S., Snapp, E. L., Cole., N. B., Zaal, K. J., Kenworthy, A. K., Roberts, T. H., Ellenberg, J., Presley, J. F., Siggia, E., and Lippincott-Schwartz, J. (2000) *Nat. Cell Biol.* **2,** 288–295
30. Bannykh, S. I., Bannykh, G. I., Fish, K. N., Moyer, B. D., Riordan, J. R., and Balch, W. E. (2000) *Traffic* **1,** 852–870
31. Helenius, A., and Aebi, M. (2001) *Science* **291,** 2364–2369
32. Bebök, Z., Mazzochi, C., King, S. A., Hong, J. S., and Sorscher, E. J. (1998) *J. Biol. Chem.* **273,** 29873–29878
33. Tatu, U., and Helenius, A. (1997) *J. Cell Biol.* **136,** 555–565
34. Szczesna-Skorupa, E., Chen, C.-D., Rogers, S., and Kemper, B. C. (1998) *Proc. Natl. Acad. Sci. U. S. A.* **95,** 14793–14798
35. Cole, N. B., Smith, C. L., Sciaky, N., Terasaki, M., Edidin, M., and Lippincott-Schwartz, J. (1996) *Science* **273,** 797–801
36. Marguet, D., Spiliotis, E. T., Pentcheva, T., Lebowitz, M., Schneck, J., and Edidin, M. (1999) *Immunity* **11,** 231–240